Title:

Loss of ubiquitinated protein autophagy is compensated by persistent CncC/Nrf2 antioxidant responses

Running title: p62 mitigates oxidative stress in flies

Arindam Bhattacharjee[1,6], Adél Ürmösi[1,2,6], András Jipa[1], Levente Kovács[4,5], Péter Deák[4], Áron Szabó[1], Gábor Juhász[1,3,*]

[1]Institute of Genetics; Biological Research Centre; Szeged, H-6726; Hungary.

[2]Doctoral School of Biology; University of Szeged; Szeged, H-6720; Hungary.

[3]Department of Anatomy, Cell and Developmental Biology; Eötvös Loránd University; Budapest, H-1117; Hungary.

[4]Department of Genetics, University of Szeged, Szeged, H-6720; Hungary.

[5]present address: Division of Biology and Biological Engineering, California Institute of Technology, Pasadena, CA, USA.

[6]These authors contributed equally

[*]Correspondence to: gabor.juhasz@ttk.elte.hu

1

Keywords:

autophagy, autophagic receptor, Drosophila, longevity, oxidative stress

Abbreviations

Atg8a: autophagy-related 8a; Cnc: cap-n-collar; IFM: indirect flight muscle; Keap1: kelch-like ECH associated protein 1; LIR: LC3-interaction region; Nrf2: Nuclear factor (Erythroid-derived 2)-like 2; PB1: Phox and Bem1; Ref(2)P: refractory to sigma-P; SAR: selective autophagy receptor; UBA: ubiquitin-associated;

Abstract (250 word limit)

P62-type selective autophagy receptors cross-link poly-ubiquitinated cargo and autophagosomal LC3/Atg8 proteins to deliver them for lysosomal degradation. Consequently, loss of autophagy leads to accumulation of polyubiquitinated protein aggregates that are also frequently seen in various human diseases, but their physiological relevance is incompletely understood. Here, using a genetically non-redundant *Drosophila* model, we show that specific disruption of ubiquitinated protein autophagy and concomitant formation of polyubiquitinated aggregates has hardly any effect on bulk autophagy, proteasome activity and fly healthspan. We find that accumulation of Ref(2)P/p62 due to a mutation that disrupts its binding to Atg8a results in the co-sequestering of Keap1 and thus activates the CncC/Nrf2 antioxidant pathway. These mutant flies have increased tolerance to oxidative stress and reduced levels of aging-associated mitochondrial superoxide. Interestingly, ubiquitin overexpression in Ref(2)P point mutants prevents the formation of large aggregates and restores the cargo recognition ability of Ref(2)P, although it does not prevent the activation of antioxidant responses. Taken together, potential detrimental effects of impaired ubiquitinated protein autophagy are compensated by the aggregation-induced antioxidant response.

Introduction

Macroautophagy (autophagy hereafter) is an evolutionarily conserved catabolic process for lysosomal degradation of cellular cargo. In this process, a double-membrane vesicle known as autophagosome engulfs cellular cargo and eventually fuses with lysosomes for degradation. Unlike

bulk autophagy where cargo engulfment is at random, recognition of specific cargo is a key feature of selective autophagy. Selective autophagy receptors (SARs) bridge the gap between recognition of cargo and its subsequent targeting to the autophagosome. Thus, two key features of all SARs include first, selective cargo capture, and second, binding to autophagosomal membrane-resident LC3 (microtubule-associated protein 1 light chain 3)/Atg8 family proteins. Binding of SARs to LC3 is mediated by an 'LC3-interaction region' (LIR), which recognizes complementary binding sites on LC3 known as LIR-docking site [1]. Functionally, SARs can be immobile, such as organelle-bound SARs (e.g. FUNDC1, FAM134B), or soluble (e.g. p62, NBR1). The latter type is also known as sequestosome-1-like receptors (SLRs) after its flagship member p62/SQSTM1 [2,3].

Apart from the LIR, p62 has a N-terminal Phox and Bem1 (PB1) domain mediating its oligomerization, a C-terminal ubiquitin-associated (UBA) domain for recognizing polyubiquitinated cargo and a Keap1-interaction region (KIR) [4]. PB1-mediated oligomerization of cargo-bound p62 can promote phase separation from the cytosol into membraneless gel-like structures, a process accelerated by polyubiquitin [5–8]. The KIR motif meanwhile is responsible for binding to the Kelch-like ECH-associated protein 1 (Keap1), which is an adapter for the E3 ligase Cullin 3. Keap1 facilitates degradation of the transcription factor Nuclear factor erythroid 2–related factor 2 (Nrf2) as part of the Cullin3-Keap1-Nrf2 complex. During oxidative stress, the Keap1-Nrf2 interaction is perturbed by oxidation-sensitive cysteine residues on Keap1 and also by p62 through KIR-Keap1 interaction and subsequent autophagic degradation of Keap1. In such conditions, free Nrf2 is able to promote the transcription of antioxidant response element (ARE)-containing genes to mount the oxidative stress response [4,9]. The *Drosophila* homolog of p62

(also known as Ref(2)P) has a similar domain structure and it is the sole known autophagy receptor for ubiquitinated proteins in flies. Thus, Ref(2)P mutants present a non-redundant model to study selective ubiquitin autophagy defects. While Ref(2)P ΔPB1 and ΔUBA mutants were found to suppress aggregate formation in the brain of Atg8a mutant flies [10], it left the important question open: what is the consequence of specifically disrupting the autophagic turnover of ubiquitinated proteins without affecting their aggregation and leaving bulk autophagy functional?

Here we reveal using the first in vivo Ref(2)P LIR mutation that impaired selective autophagy of ubiquitinated proteins has no effect on bulk autophagy and proteasome function and only minimally affects fly healthspan, despite the dramatic accumulation of ubiquitinated aggregates. We find that Keap1, a negative regulator of antioxidant gene expression, is also captured into Ref(2)P-positive polyubiquitinated aggregates that results in elevated CncC/Nrf2 activity and thus increased tolerance of oxidative stress. Lastly, we show that aging-associated mitochondrial superoxide production is attenuated by this ectopic CncC signaling in Ref(2)P LIR mutant flies. Our study clearly shows that I. ubiquitinated protein degradation by autophagy is not critical for normal animal physiology, II. massive accumulation of protein aggregates is well-tolerated on both cellular and organismal levels, III. potential consequences of the lack of ubiquitinated protein autophagy are compensated by the gain of Nrf2 function.

Results

Disrupting the LIR of *Drosophila p62/Ref(2)P* results in the formation of ubiquitinated protein aggregates

The LIR motif is characterized by the consensus sequence Θ_0-X_1-X_2-Γ_3 (core LIR). The Θ_0 aromatic (W/F/Y) and Γ_3 aliphatic (L/I/V) residues bind to the two hydrophobic pockets of the LIR docking site on the surface of Atg8 family proteins, respectively, while upstream acidic residues stabilize this interaction and are part of the 'extended LIR' [11,12]. *Drosophila* p62/Ref(2)P has a single LIR with a core sequence W^{454}-Q-L-I^{457}. Biochemical analyses revealed that the two alanine substitutions W454A, I457A in the LIR are sufficient to prevent Ref(2)P-Atg8a interaction and therefore its lysosomal delivery *in vitro* [13]. We sought to explore the physiological consequences of this mutation in flies. To that end, we generated a *Drosophila* knock-in mutant for Ref(2)P with the above amino acid changes (W454A, I457A, hereafter referred to as *Ref(2)P^{LIRm}*, Figure 1A). The Ref(2)P-Atg8a interaction was indeed abolished in the mutants (Figure 1B) and as a consequence these flies accumulated large amounts of Ref(2)P and poly-ubiquitin compared to control whole-fly lysates (Figure 1C).

Accumulated Ref(2)P was found to be systemically present in poly-ubiquitin (poly-Ub)-positive aggregates in the larval fat cells, adult brain and thoracic indirect flight muscles (IFM); meanwhile no increase in cytoplasmic Ref(2)P signal was observed. In larval fat tissue, there were significantly more such poly-Ub and Ref(2)P positive aggregates in mutants than in controls (Figures 1D and 1E). Ref(2)P signal strongly colocalized with poly-Ub in the *Ref(2)P^{LIRm}* brain and this colocalization increased with age (Figures 1F-1H). This suggests that ubiquitinated proteins, which are normally mostly present in soluble form and turned over by selective

autophagy, are rapidly sequestered into insoluble Ref(2)P aggregates in our LIR mutants. This is also in agreement with the increased poly-Ub signal in 3-day-old $Ref(2)P^{LIRm}$ whole-fly lysates. We next used electron microscopy to better characterize these structures in optic lobe cortical neurons. We saw that the aggregates are cytosolic, membraneless structures of ~0.5-4 μm in diameter (Figure 1I).

Notably, loss of *Atg* gene function such as *Atg7*, *Atg8a* or *Atg16*, also results in accumulation of Ref(2)P-positive neuronal protein aggregates [10,14,15]. We introduced one such mutation: $Atg16^{d129}$ into the $Ref(2)P^{LIRm}$ background, and no further increase in the number of Ref(2)P-positive structures or total Ref(2)P accumulation was seen (Figure 1J and 1K), which also supports the complete elimination of selective ubiquitin/Ref(2)P autophagy by the LIR mutation. Together, these results indicate rapid co-sequestration of polyubiquitinated proteins and Ref(2)P as a result of blocking selective autophagic flux.

$Ref(2)P^{LIRm}$ flies retain normal bulk autophagy and proteasomal function

p62 aggregates can serve as autophagosome nucleation sites by direct interaction with FIP200, a subunit of the autophagy initiating ULK1 kinase complex [16]. We therefore asked whether bulk autophagy is affected by the Ref(2)P LIR mutation. Firstly, no significant difference in the number of lysotracker-positive structures (labeling acidic autolysosomes in larval fat cells) and lipidated Atg8a levels were observed between starved control and $Ref(2)P^{LIRm}$ L3 larvae after starvation (Figures S1A-S1D). We also saw identical starvation responses in control and mutant starved larval fat tissue using an endogenous promoter-driven 3xmCherry-Atg8a reporter [17] (Figures

S1E and S1F). Finally, starvation did not further increase the number of Ref(2)P punctae in *Ref(2)P^{LIRm}* fat tissue (Figures S1G and S1H). Collectively, loss of Ref(2)P degradation does not impair bulk autophagy.

Since LIR mutants had widespread proteostasis defects, we decided to also analyze proteasomal activity. In autophagy-deficient HeLa cells, proteasomal substrates were found to accumulate due to impaired delivery to the 26S proteasome [18]. In contrast, we did not see any difference in the expression of the *Drosophila* 26S proteasomal subunits in control versus *Ref(2)P^{LIRm}* flies (Figure S2A) and the levels of two different proteasomal targets did not change either. First, levels of the proteasomal cargo pim/securin were similar in *Ref(2)P^{LIRm}* and control whole-fly lysates (Figure S2B). Second, we used the CL1-GFP reporter, which is a GFP-tagged proteasome-specific degron that is rapidly degraded by the ubiquitin-proteasome system [19]. Again, the levels of GFP-CL1 signal in 30-day old *Ref(2)P^{LIRm}* brains exhibited no obvious difference compared with control (Figures S2C and S2D). These data corroborate the previous observation that p62/Ref(2)P accumulation by itself does not result in significant changes of proteasomal function [18]. Thus, proteasomal activity is unperturbed despite the extensive proteostasis defects.

Ref(2)P^{LIRm} flies do not show severe physiological defects, but they are more resistant to paraquat-induced oxidative stress

Proteotoxic stress is typically associated with decreased lifespan [20]. We have shown earlier that multiple *Atg* mutants including *Atg7^{d77}* and *Atg16^{d67}* have significantly shortened lifespan [14,15]. Ref(2)P ΔPB1 and ΔUBA mutant flies (*Ref(2)P^{od2}* and *Ref(2)P^{od3}*, respectively), were also

reported to have slightly shorter lifespan, clearly reduced locomotor function and slightly increased susceptibility to oxidative stress induced by paraquat (PQ), a putative Parkinson Disease-causing agent [21]. On the other hand, p62 overexpression reduces proteostasis defects and increases lifespan in flies and worms [22,23]. We decided to isogenize our mutant lines to eliminate differences in genetic backgrounds that can strongly influence lifespan [24]. Surprisingly, isogenic *Ref(2)P^LIRm* flies had only a minimally shortened lifespan in well-fed (14% reduction of median lifespan in *Ref(2)P^LIRm*) and no difference under complete starvation conditions compared to isogenic control flies (Figures 2A and 2B). Moreover, climbing activity, a measure of neuromuscular performance, was similar to control flies at both 3- and 30-day ages (Figure 2C). Strikingly, 3-day old *Ref(2)P^LIRm* flies demonstrated significantly increased tolerance to PQ-induced oxidative stress compared to controls when fed with 20 mM PQ until death (66% increase in median survival for *Ref(2)P^LIRm*; Figure 2D). Incidentally, both PB1 and UBA domains of Ref(2)P are required for formation of ubiquitinated protein aggregates in the brain, thus *Ref(2)P^od2* and *Ref(2)P^od3* flies are unable to form poly-Ub positive Ref(2)P aggregates [10]. The results here thus establish a link between aggregate formation and associated physiological changes in Ref(2)P LIR mutants.

Paraquat resistance is driven by Keap1 sequestration and CncC/Nrf2 activation

In mammals, p62 phase separation into aggregates can sequester Keap1, leading to ectopic activation of Nrf2 and a downstream antioxidant response via increased transcription of oxidative stress response genes. The canonical Keap1-p62 interaction via p62 KIR and Keap1 'Double glycine repeat and C-terminal' (DC) region is altered in flies since Ref(2)P appears to lack a KIR

[4]. Nonetheless, others and we have shown that Ref(2)P co-immunoprecipitates with ubiquitinated dmKeap1 that is mediated by the Ref(2)P UBA domain, and deletion of the UBA domain, but not the LIR mutation (W454A/I457A) abolishes this interaction [13,25]. We therefore tested whether ubiquitinated Keap1 might be co-sequestered with Ref(2)P aggregates. Indeed, when GFP-dmKeap1 was expressed with a pan-neuronal *nSyb* driver, LIR mutant adult brains accumulated significantly more GFP-dmKeap1 puncta, and these punctate structures partially colocalized with Ref(2)P (Figures 3A and 3B). Similar results were observed in the case of endogenous dmKeap1 and Ref(2)P (Figure S3). Corroborating this, whole-fly lysates from 3-day old *Ref(2)P^{LIRm}* flies had more endogenous Keap1 than controls did (Figures 3C and 3D). Since Keap1 sequestration is known to activate CncC/Nrf2, we next studied CncC activation as a possible route for PQ tolerance in our mutants. We found that *Ref(2)P^{LIRm}* flies indeed had increased transcriptional activity of *CncC* and downstream ARE-containing targets including *Keap1* itself, *glutathione-S-transferase E1* (*GstE1*) and *catalase*. Notably, *Ref(2)P* transcription in the mutant flies remained unaltered (Figure 3E). Consistent with this, we saw increased nuclear translocation of CncC in the larval midgut cells of *Ref(2)P^{LIRm}* flies (Figures 3F and 3G). We reasoned that if PQ tolerance in *Ref(2)P^{LIRm}* flies is indeed CncC-mediated, loss of CncC function should abolish this. Indeed, silencing *CncC* in *Ref(2)P^{LIRm}* mutants completely suppressed the PQ resistance: these flies had 33% reduction in median PQ survival compared to *Ref(2)P^{LIRm}* mutants (Figure 3H). Thus, CncC/Nrf2 is upregulated due to Keap1 sequestration in Ref(2)P aggregates and PQ tolerance is an unexpected gain-of-function effect in our selective ubiquitin autophagy mutant flies.

Aging associated mitochondrial superoxide production is ameliorated by elevated CncC/Nrf2

Aging-associated production of superoxides in thoracic muscle mitochondria was earlier shown to be reversed by Ref(2)P overexpression starting in mid-life as well as by overexpressing the mitochondrial fission factor Drp1, both of which accelerated mitochondrial degradation [22,26]. In the case of our mutants, we reasoned that aging-associated superoxide production might be ameliorated by increased CncC activity. Indeed, we observed a marked reduction of Mitosox red signal in optic lobe of brains of 45-day old LIR mutant flies compared to controls, which measures mitochondrial superoxide levels (Figures 4A and 4B). Similar results were also observed in 45-day old IFMs (Figure S4A and S4B). Supporting that this effect is indeed due to ectopic CncC activity, we found that mitochondrial superoxide levels in 45 day old tissues expressing CncC RNAi in either control or *Ref(2)P^LIRm* backgrounds were comparable to each other (Figures 4A-B, S4A-B).

Disrupting aggregate formation redirects excess Ref(2)P to mitochondria during mitophagy

Our next aim was to see whether aggregate formation of Ref(2)P was essential for its inhibitory effect on Keap1. To address this, we generated a fly stock expressing UAS-driven N-terminally GFP-tagged monoubiquitin and subsequently overexpressed it with the strong, ubiquitous *tubulin* driver in Ref(2)P^LIRm. Overexpression of tetra-ubiquitin chains have been shown to disrupt the p62-ubiquitin crosslink by increasing p62 zinc finger (ZZ)−ubiquitin interaction in monomeric p62, and thus reducing PB1-mediated formation of helical p62 polymers [5,27]. In line with past

observations, we found that first, Ref(2)P^{LIRm}; *tub*>GFP-Ub tissue had markedly less Ref(2)P aggregates than Ref(2)P^{LIRm} animals, and had a strong reduction of Ref(2)P puncta size in both larval fat tissue and adult brain (Figure 5A-C). Notably, the robust colocalization of Ref(2)P with endogenous ubiquitin decreased, leading to smaller Ref(2)P-positive clusters mostly being devoid of ubiquitin signal (Figure 5D). This indicates that Ref(2)P-ubiquitin co-sequestration is essential for growth of these aggregates. Second, *tub*-GFP-Ub expression increased the number of GFP-Ub puncta in Ref(2)P^{LIRm} but not in control, indicating that excess undegraded Ref(2)P promotes ubiquitin cluster formation (Figure S5A-B). Surprisingly, ubiquitin-positive Keap1 puncta were still observed in Ref(2)P^{LIRm}; *tub*>GFP-Ub tissue, suggesting that the UBA-mediated Keap1-Ref(2)P interaction is not strictly dependent on Ref(2)P aggregate formation (Figure S5C). As a result, these flies had comparable PQ tolerance and *cnc* mRNA levels to Ref(2)P^{LIRm} (Figure S5D-E). Of note, the increased nuclear translocation of CncC seen in Ref(2)P^{LIRm} animals was still observed in the *tub*-GFP>Ub background (Figure S5F-G).

Ref(2)P is found on undegraded mitochondria during aging and its overexpression accelerates mitophagy [22,26]. The presence of many small Ref(2)P dots in *tub*-GFP-Ub; Ref(2)P^{LIRm} tissue raised the possibility that non-aggregated Ref(2)P can now be directed to ubiquitinated cargo recognition as required. To test this, we fed larvae with CCCP to induce mitophagy, which leads to outer mitochondrial membrane protein ubiquitination for selective autophagic degradation. We found increased mitochondrial localization of Ref(2)P in Ref(2)P^{LIRm}; *tub*>GFP-Ub tissue, whereas in Ref(2)P^{LIRm} cells the mitochondrial localization of Ref(2)P was significantly less frequent (Figure 5E-F).

Discussion

To examine the consequences of selective ubiquitinated protein autophagy defects and large-scale aggregate formation in a complete animal, we disrupted the LIR of their only known receptor Ref(2)P/p62 in *Drosophila*. The lack of any obvious proteotoxicity in this mutant is striking and can likely be attributed to most polyubiquitinated cargo being co-sequestered in phase-separated liquid droplets [6,8]. We find that these poly-Ub aggregates contain Keap1, a negative regulator of the CncC/Nrf2-dependent oxidative stress response. Keap1 autophagic degradation in flies is facilitated by Ref(2)P through its LIR-mediated interaction with Atg8a-Keap1 complex, which promotes engulfment of the resulting aggregates. Thus, free Keap1 levels and by extension, Nrf2 activity is regulated by Ref(2)P similar to mammals [13]. An important consequence of the Ref(2)P-Keap1 co-sequestration in the LIR mutant is persistently elevated Nrf2 activity as its proteasomal degradation is prevented, ultimately leading to increased PQ tolerance (Figure 5G). Our results explain the increased PQ susceptibility seen in ΔPB1 and ΔUBA mutants of Ref(2)P, which are due at least in part to their cargo (including Keap1) sequestration defects.

We find that persistent Nrf2 activation in our p62-LIR mutants can have physiological benefits even compared to wild type animals. In this model, sequestration of ubiquitinated cargo firstly decreases their proteotoxicity. Second, Nrf2-mediated increased detoxification likely reduces the burden of ubiquitinated proteins, which may also reduce the levels of soluble, presumably more toxic species. It is important to emphasize that *Atg* mutant flies and other animals develop a collection of physiological defects including neurodegeneration, ataxia and very short lifespan

[10,14,15,28], but the relative contributions of bulk and selective ubiquitin-mediated autophagy are difficult to establish in these cases. However, our selective ubiquitinated protein autophagy defective flies develop just as many poly-Ub aggregates as *Atg* mutants do, but they do not show any major physiological defects. We note that we carried out all of our experiments on a *white* mutant background. As loss of this ABC transporter was shown to influence folate metabolism [29], we cannot exclude the possibility that this might influence protein aggregation in the genotypes that we studied. Supporting our *Drosophila* data, overexpression of a synthetic LIR peptide in mouse liver to competitively inhibit the engagement of p62 and likely other binding partners of LC3 was recently reported to cause accumulation of p62 aggregates that led to persistent Nrf2 activity, while bulk autophagy remained intact and liver dysfunction that is typical in autophagy mutants was not seen either [30].

Persistent antioxidant gene expression in *Ref(2)P^LIRm* flies appears to reduce the oxidative damage of organelles such as mitochondria, too. Consistent with this, mitochondrial superoxide production was reduced by constitutively active Nrf2 in our LIR mutants. Of note, *Keap1* mutant heterozygotes live longer and also have higher PQ tolerance than wild type flies [31]. However, based on our longevity experiments carried out on an isogenic background, *Ref(2)P^LIRm* flies still have a slightly shorter lifespan than control flies do, which may be due to an increased dependency on ubiquitin-mediated selective autophagy during aging [32]. Additionally, the gradual conversion of dynamic liquid droplets into inclusions containing aggregates of Ref(2)P and ubiquitinated proteins may also contribute to the lifespan defect [33]. We therefore reason that the degradative flux of selective autophagy plays a critical role in long-term survival or later in life, loss of which ultimately outweighs the benefits of Nrf2-mediated increased detoxification. Notably,

overexpression of ubiquitin was able to disrupt aggregate formation *in vivo*, although ubiquitin-positive Keap1 aggregates still formed. In this mutant, due to the unique overabundance of undegraded Ref(2)P and overexpressed ubiquitin, Ref(2)P-UBA mediated interaction with ubiquitin appears to be impaired, leading to a pool of ubiquitin-unbound cytosolic Ref(2)P, which can still oligomerize. This non-sequestered Ref(2)P seems able to nucleate the excess ubiquitin from cytosol into small aggregates, but also able to perform its UBA-associated tasks such as Keap1 sequestration and mitochondrial localization during mitophagy. We performed fluorescence recovery on GFP-Ub aggregates formed in the *tub*-GFP-Ub; LIR mutant tissue to find that recovery was not significant, unlike p62 and tetra-ubiquitin chain-induced aggregates that rapidly recover their ubiquitin fluorescence [5]. This indicates that the aggregates lose their dynamic nature after crosslinking with cellular ubiquitinated cargo, and Keap1 sequestration might not be reversible in the presence of excess Ref(2)P.

In summary, we show that the lack of autophagic clearance of ubiquitinated proteins and their resulting massive aggregation is physiologically well tolerated due to compensation by increased antioxidant responses. It is important to note that without Nrf2 gain-of-function, selective ubiquitinated protein autophagy mutants in which aggregate formation is also prevented (that is, Ref(2)P mutants lacking the PB1 or UBA domains, respectively) were reported to show clearly impaired locomotor activity [21]. This highlights the protective role of cargo sequestration and associated signaling events.

Materials and Methods

Antibodies and reagents

Primary antibodies: HA (WB 1:1500; Roche 11867431001), Alpha-tubulin (mouse; WB 1:2000; DSHB , AA12.1), GFP (chicken; IF 1:500; Aves Labs, Inc., GFP-1020), 26S proteasome cocktail containing α- p54, α- p48A, α- p42A, α- p39A, α- CPα7 (mouse; WB 1: 2000; Zoltán Lipinszki), dmKeap1 (rabbit; IF 1:250, WB 1:1000; Terje Johansen), Ref(2)P (rabbit; IF 1:300, WB 1:2000) [34], poly-ubiquitin FK2 (mouse; IF 1:350, WB 1:1000; Enzo, BML-PW8810), GABARAP (rabbit; IF 1:400, WB 1:2000; Abcam, ab109364), mCherry (mouse; WB 1:1000, Novus Biologicals, NBP1-96752), CncC (rabbit; IF 1:10; Huai Deng) [35]. Secondary antibodies for IF: goat anti-rabbit Alexa Fluor 488 (Invitrogen, A-11008), goat anti-rabbit Alexa Fluor 546 (Invitrogen, A-11010), goat anti-mouse Alexa Fluor 488 (Invitrogen, A-11001), goat anti-mouse Alexa Fluor 546 (Invitrogen, A-11003), goat anti-chicken DyLight 488 (Thermo Scientific, SA5-10070) [all 1:800]; for WB: IRDye 800CW goat-anti rabbit (LI-COR Biosciences, 926-32211), 800CW goat anti-mouse (LI-COR Biosciences, 926-32210), 680RD goat-anti mouse (LI-COR Biosciences, 926-68070) [1:5000]. Reagents: Lysotracker red (Invitrogen, L7528), paraquat (Sigma, 36541), DAPI (Sigma, D9542), Laemmli sample buffer (Sigma, S3401), DirectZol RNA Miniprep kit (Zymo Research, R2051), RevertAid First Strand cDNA Synthesis Kit (Thermo Scientific, K1622), Odyssey TBS blocking buffer (LI-COR Biosciences, 927-50000), RFP-Trap Magnetic Agarose (Chromotek, rtma-20).

Fly stocks and maintenance

Fly stocks: w[1118] (BDSC: #5905), 3×mCherry-Atg8a [17], w[*]; P{w[+mC]=sqh-EYFP-Mito}3 (BDSC: #7194), Cnc RNAi [TRiP.HMS00650]/TM3, Sb (BDSC: #32863), p[w+ 9×pim-2.HA] 3.2 (Zoltan Lipinszki), UAS-GFP-CL1 [19], y[1] w[*]; P{w[+m*]=nSyb-GAL4.S}3 (BDSC: #51365), Atg16[d67] and Atg16[d129] [15], UAS-GFP-Keap1/FM7, UAS-GFP-Keap1/CyO and UAS-GFP-CncC-7/TM3 (Terje Johansen), Tub-GAL4/TM6. Flies were reared on standard yeast/cornmeal agar medium in glass vials at 25 °C. Third instar feeding larvae and three-day old adults were used for all experiments unless otherwise stated.

Generation of Ref(2)P LIR mutant and GFP-Ubiquitin flies

Following a previous protocol [36], the Ref(2)P[LIRm] stock was generated using CRISPR/Cas9 homology-directed repair to replace the endogenous LIR. The gRNA sequences were cloned into BbsI sites of pCFD5 plasmid using the oligonucleotides: Ref2Guide3F: tgcaTTGTCAATAAGCTGCCACTC and Ref2Guide3R: aaacGAGTGGCAGCTTATTGACAA (Addgene #73914). This guide RNA carrier clone was co-injected into Act5C-Cas9, lig4169 fly eggs together with a ssDNA template containing two homologous arms and the desired change: AGTGGGATTGGTTGTGTCCAGATTGATCAAGTTACTATTGTTTGCAGAGTATGCATT GTCGGCCAGCTGGGCCTCTGGATCCAAGCTGTCTGAACGGCGTCTTTCCTGCTCTGTT TCGGTGGTGGTTTCCGA. Insert was verified with Sanger sequencing. Mutants were identified with Sanger sequencing using LIR mutation-specific primers, and also for total Ref(2)P accumulation in Western blot. Sequencing primers, donor ssDNA sequences are listed on Table S1. Mutant flies were isogenized by 6 times repeated backcrossing with isogenic w[1118] stock.

Gateway® system (Invitrogen) was applied to generate the UAS-GFP-Ub construct. First, 289 bp of mono-ubiquitin coding sequence was cloned into DraI/EcoRI sites of pENTR3C™ (Invitrogen) entry vector. pENTR3C-Ub plasmid was used in a LR reaction to incorporate mono-Ub coding sequence into pTGW *Drosophila* expression vector providing UAS recognition sequence and N-terminal GFP tag. An attB site was introduced into the EcoR47III restriction site of pTGW prior to the LR reaction. The resulting pTGWattB-Ub plasmid was injected into flies carrying a nos-phiC31 integrase and P{y$^+$CaryP}attP2 landing site on the 3rd chromosome. Transformant flies carrying UAS-GFP-Ub were identified based on their non-white eye color.

Lifespan analysis and paraquat resistance

For lifespan analysis, newly hatched flies were collected and maintained at a density of 20 flies/vial in a humidified incubator at 25°C in standard food. Flies were moved to fresh vials thrice a week and the number of dead flies were recorded. For complete starvation, flies were kept in empty vials with only a soaked filter paper as a water source, which was replaced daily until they died. Number of dead flies were recorded every 12 h.

For paraquat resistance, 3-day old flies were kept in vials at a density of 20 flies/vial and containing a filter paper soaked in 20 mM paraquat (PQ). Flies were transferred to fresh vials containing PQ every 24 h until dead and the number of dead animals was recorded every 12 h.

Climbing assay

Following a previous protocol [26], flies were anesthetized with CO_2 and put in a 100 ml graduated cylinder (height=249 mm) as a climbing chamber. Flies were allowed to recover, afterwards the cylinder was tapped down and the flies were allowed to climb for 2 minutes. This process was repeated eight more times. One minute after the last tap, an image was recorded and the number of flies in top, middle and bottom 1/3rd regions were counted.

Electron microscopy

Electron microscopy was performed following protocol described earlier [37]. Briefly, 3-day old adult female brains were dissected in PBS and fixed in 3.2% paraformaldehyde, 0.5% glutaraldehyde, 1% sucrose, 0.028% $CaCl_2$ in 0.1 N Na-cacodylate buffer (pH=7.4) overnight at 4 °C, postfixed in 0.5% OsO_4 for 1 h, and embedded in Araldite. 70 nm ultrathin sections were obtained and stained with Reynold's lead citrate. Imaging was done on a Jeol JEM-1011 transmission electron microscope equipped with Olympus Morada camera at 5,000-10,000× magnification.

Lysotracker red and MitoSOX red staining

L3-mid larvae were starved by floating in a 20% sucrose solution in PBS for 4 h. Larval fat tissue from starved larvae were dissected in PBS, stained immediately in a cocktail of 50 nM Lysotracker red and 0.5 µg/ml DAPI in PBS for 4 minutes. Thereafter, the samples were washed once in PBS, mounted in glass slides with glycerol-PBS (4:1) and imaged immediately in a Zeiss Axioimager M2 system fitted with a 40×/0.75 Plan-Neofluar objective with an Apotome2 module. Number of

LTR-positive structures were counted in Fiji (NIH) by first thresholding the images and using the 'Analyze Particles' function. This was divided by nuclear (DAPI) count to get LTR dots/cell.

For MitoSOX red staining, adult female hemithoraces were dissected in cold PBS and stained with a cocktail of MitoSOX red (5 µM) and Mitotracker Green-FM (100 nM) in PBS for 12 minutes at room temperature. Subsequently, the samples were washed thrice briefly to remove unbound dye, mounted in glass coverslips with 80% glycerol-PBS and imaged immediately as described above. Mitosox fluorescence intensity was measured using Fiji in per unit area of tissue that had Mitotracker signal coverage.

Quantitative real-time PCR

3-day old flies (9 male and 9 females; in triplicate) of indicated genotype were collected and total RNA was isolated using DirectZol RNA Miniprep kit following manufacturer protocol. cDNA synthesis was carried out 1µg of total RNA with random hexamer primers and RevertAid cDNA synthesis kit following manufacturer protocol. The following settings were used for synthesis: 25°C for 5 minutes, 42°C for 60 minutes and 72°C for 5 minutes. 50 ng of cDNA in three biological and three experimental replicate each was used for quantitative real-time PCR using PerfeCTa SYBR Green FastMix (QuantaBio) in a Qiagen Rotor-Gene Q system using following conditions: initial denaturation (95°C for 5 min), followed by 45 cycles of 95°C for 20 seconds, 60°C for 20 seconds and 72°C for 20 seconds, with a melt curve of 55-95°C at 0.33°C per step. Specificity of the amplified products was confirmed by melting curve analysis. Quantification of data was performed in Rotor-Gene-Q software (Qiagen) using the $2^{-\Delta\Delta CT}$ method and gene expression was normalized against rpl32. Primers are listed on Table S1.

Immunocytochemistry and image analysis

Freshly dissected tissue (L3 larval fat tissue, N≥8; adult hemithoraces, N≥10; or adult brain, N≥6) were fixed with 4% paraformaldehyde in PBS for 30 minutes, washed thrice in PBTx buffer (PBS supplemented with 0.1% Triton-X 100 for fat tissue and 0.3% for brain samples) for 10 minutes each and followed by blocking in 5% normal serum in PBTx for 1h at room temperature (4h for adult brain). Tissues were then incubated in primary antibody solution of PBTx containing 5% serum overnight (2 overnights for adult brain) at 4°C with gentle rocking. This was followed by washing thrice in PBTx (0.1% Triton-X 100 for fat tissue; 0.3% for brain) and incubation with secondary antibodies in the PBTx-5% serum solution for 2h at room temperature with gentle rocking (overnight at 4°C for adult brain). Afterwards, the tissues were again washed thrice with PBTx as before, incubated with DAPI solution for 15-20 minutes, washed once with PBS and mounted in a glass slide with 80% glycerol in PBS. Imaging was done with a Zeiss Axioimager M2 system as described above. For counting of Ref(2)P puncta, images were thresholded to remove background noise and particles were analyzed in red channel [Ref(2)P; particle size ≥ 0.2 μm^2] and blue (DAPI) channel using the 'Analyze Particles' function in Fiji (NIH). Similarly, to measure the size of puncta, images were thresholded and 'Analyze Particles' function was used. For colocalization analyses, minor adjustment to brightness and contrast of whole images were made to remove any background fluorescence; ROI containing the signal was cropped and processed through the 'Coloc 2' plugin in Fiji and a Pearson's correlation coefficient (r) above threshold was considered with a Costes randomization of 50.

Co-immunoprecipitation (Co-IP) and Western blot (WB)

For coimmunoprecipitation of endogenous Ref(2)P and 3xmCherry-Atg8a, 130 1-7 days old whole flies were used for extraction. Flies were homogenized in a Dounce homogenizer using 45 strokes with a pestle in 1.5 ml of ice-cold Homogenization Buffer (HB): 20 mM HEPES pH=7.5, 150 mM NaCl, 1 mM EDTA, 0.2% Triton X-100 and protease inhibitor cocktail (Pierce Protease Inhibitor Tablet, Thermo Scientific). Crude lysates were centrifuged twice, first to eliminate fly debris (5 min, 1000 g, 4 °C) and then to deplete the lysate from insoluble aggregates (15 min, 58000 g, 4 °C). 25 μl equilibrated RFP-Trap Magnetic Agarose was incubated with 1 mg of fly extract for 3 hours with rotation at 4 °C. Beads were washed three times for 10 minutes each in 1 ml of HB at 4 °C. Elution was done with 50 μl of 1x Laemmli sample buffer containing 100 mM DTT by boiling for 5 min at 100 °C. 25 μl of eluate was loaded on gels along with 20 μg of inputs. For WB, anti-mCherry at 1:1000 and anti-Ref(2)P at 1:1000 were used.

For WB of whole animal lysates, L3 larvae or adults were directly boiled with 1x Laemmli sample buffer to inactivate proteases, homogenized with a plastic pestle, boiled again for 5 minutes and spun down to remove debris. Equal amount of protein was loaded in SDS-polyacrylamide gels and transferred to a 0.45 μm PVDF membrane (Immobilon-FL, Millipore) overnight. Membranes were blocked with TBS Odyssey blocking buffer for 1h at room temperature, followed by incubation with primary antibodies for overnight at 4°C. Membranes were washed four times (5 minutes each) in TBST (TBS containing 0.1% Tween-20) buffer after primary antibody incubation and incubated in appropriate secondary antibodies for 1.5 h at room temperature. Then, membranes were washed thrice in TBST buffer for 5 minutes each, briefly washed once with TBS and dH2O each, and

finally imaged in a LI-COR Odyssey CLx system. Band density was analyzed with Image Studio software (LI-COR Biosciences). Antibodies were diluted in TBS Odyssey blocking buffer or TBS+2.5% non-fat milk + 2.5% BSA, supplemented with 0.1% Tween-20 (additionally 0.01% SDS was added for secondary antibodies).

Statistical analysis

Statistical analysis was performed in GraphPad Prism 6. All ROI (regions of interest) selections were random sections from the image that showed fluorescence after applying a square grid overlay. Unpaired two-tailed Student's t-test was used to compare between two groups. Welch's correction was applied when the distributions had unequal standard deviation. One-way ANOVA was used for comparison between multiple groups of datasets. Non-parametric tests (Mann-Whitney U test for two independent groups and Kruskal-Wallis test for multiple independent groups) were performed when one or more dataset did not pass Shapiro-Wilk normality test ($p>0.05$). Multiple comparisons between three or more data sets were done with Bonferroni's post-hoc test. Kaplan-Meier analysis was used for lifespan experiments, followed by Log-rank (Mantel-Cox) test. Differences were typically considered significant as ****$p<0.0001$, ***$p<0.005$, **$p<0.01$, *$p<0.05$ and n.s. $p>0.05$. Error bars represent ± standard error of mean (SEM). All experiments including co-IPs and western blots were carried out at least twice using independent biological samples.

Acknowledgements

Disclosure statement

The Authors declare that they have no conflict of interest.

Author Contributions

A.B., A.Ü., A.J., L.K., P.D., A.S., G.J. designed, performed experiments and analyzed data. G.J. conceptualized and supervised the study and acquired dedicated funding. A.B. and G.J. wrote the manuscript. All authors read, contributed to and approved of the manuscript.

Data Availability Statement

Source data supporting the findings of this study is available upon request.

References

1. Johansen T, Lamark T. Selective Autophagy: ATG8 Family Proteins, LIR Motifs and Cargo Receptors. J Mol Biol 2020; 432:80–103.

2. Bjørkøy G, Lamark T, Brech A, Outzen H, Perander M, Overvatn A, Stenmark H, Johansen T. p62/SQSTM1 forms protein aggregates degraded by autophagy and has a protective effect on huntingtin-induced cell death. J Cell Biol 2005; 171:603–14.

3. Komatsu M, Waguri S, Koike M, Sou Y, Ueno T, Hara T, Mizushima N, Iwata J, Ezaki J, Murata S, et al. Homeostatic Levels of p62 Control Cytoplasmic Inclusion Body Formation in Autophagy-Deficient Mice. Cell 2007; 131:1149–63.

4. Komatsu M, Kurokawa H, Waguri S, Taguchi K, Kobayashi A, Ichimura Y, Sou Y-S, Ueno I, Sakamoto A, Tong KI, et al. The selective autophagy substrate p62 activates the stress responsive transcription factor Nrf2 through inactivation of Keap1. Nat Cell Biol 2010; 12:213–23.

5. Zaffagnini G, Savova A, Danieli A, Romanov J, Tremel S, Ebner M, Peterbauer T, Sztacho M, Trapannone R, Tarafder AK, et al. p62 filaments capture and present ubiquitinated cargos for autophagy. EMBO J 2018; 37.

6. Sun D, Wu R, Zheng J, Li P, Yu L. Polyubiquitin chain-induced p62 phase separation

drives autophagic cargo segregation. Cell Res 2018; 28:405–15.

7. Jakobi AJ, Huber ST, Mortensen SA, Schultz SW, Palara A, Kuhm T, Shrestha BK, Lamark T, Hagen WJH, Wilmanns M, et al. Structural basis of p62/SQSTM1 helical filaments and their role in cellular cargo uptake. Nat Commun 2020; 11:1–15.

8. Yamasaki A, Alam JM, Noshiro D, Hirata E, Fujioka Y, Suzuki K, Ohsumi Y, Noda NN. Liquidity Is a Critical Determinant for Selective Autophagy of Protein Condensates. Mol Cell 2020; 77:1163-1175.e9.

9. Ichimura Y, Waguri S, Sou Y-S, Kageyama S, Hasegawa J, Ishimura R, Saito T, Yang Y, Kouno T, Fukutomi T, et al. Phosphorylation of p62 Activates the Keap1-Nrf2 Pathway during Selective Autophagy. Mol Cell 2013; 51:618–31.

10. Nezis IP, Simonsen A, Sagona AP, Finley K, Gaumer S, Contamine D, Rusten TE, Stenmark H, Brech A. Ref(2)P, the Drosophila melanogaster homologue of mammalian p62, is required for the formation of protein aggregates in adult brain. J Cell Biol 2008; 180:1065–71.

11. Birgisdottir ÅB, Lamark T, Johansen T. The LIR motif - crucial for selective autophagy. J Cell Sci 2013; 126:3237–47.

12. Noda NN, Ohsumi Y, Inagaki F. Atg8-family interacting motif crucial for selective autophagy. FEBS Lett 2010; 584:1379–85.

13. Jain A, Rusten TE, Katheder N, Elvenes J, Bruun JA, Sjøttem E, Lamark T, Johansen T. P62/sequestosome-1, autophagy-related gene 8, and autophagy in Drosophila are regulated by nuclear factor erythroid 2-related factor 2(NRF2), independent of transcription factor TFEB. J Biol Chem 2015; 290:14945–62.

14. Juhász G, Erdi B, Sass M, Neufeld TP. Atg7-dependent autophagy promotes neuronal

health, stress tolerance, and longevity but is dispensable for metamorphosis in Drosophila. Genes Dev 2007; 21:3061–6.

15.   Varga K, Nagy P, Arsikin Csordás K, Kovács AL, Hegedűs K, Juhász G. Loss of Atg16 delays the alcohol-induced sedation response via regulation of Corazonin neuropeptide production in Drosophila. Sci Rep 2016; 6:34641.

16.   Turco E, Witt M, Abert C, Bock-Bierbaum T, Su M, Trapannone R, Sztacho M, Danieli A, Shi X, Zaffagnini G, et al. FIP200 Claw Domain Binding to p62 Promotes Autophagosome Formation at Ubiquitin Condensates. Mol Cell 2019; 74:330-346.e11.

17.   Hegedűs K, Takáts S, Boda A, Jipa A, Nagy P, Varga K, Kovács AL, Juhász G. The Ccz1-Mon1-Rab7 module and Rab5 control distinct steps of autophagy. Mol Biol Cell 2016; 27:3132–42.

18.   Korolchuk VI, Mansilla A, Menzies FM, Rubinsztein DC. Autophagy Inhibition Compromises Degradation of Ubiquitin-Proteasome Pathway Substrates. Mol Cell 2009; 33:517–27.

19.   Pandey UB, Nie Z, Batlevi Y, McCray BA, Ritson GP, Nedelsky NB, Schwartz SL, Diprospero NA, Knight MA, Schuldiner O, et al. HDAC6 rescues neurodegeneration and provides an essential link between autophagy and the UPS. Nature 2007; 447:859–63.

20.   Demontis F, Perrimon N. FOXO/4E-BP signaling in Drosophila muscles regulates organism-wide proteostasis during aging. Cell 2010; 143:813–25.

21.   De Castro IP, Costa AC, Celardo I, Tufi R, Dinsdale D, Loh SHY, Martins LM. Drosophila ref(2)P is required for the parkin-mediated suppression of mitochondrial dysfunction in pink1 mutants. Cell Death Dis 2013; 4:1–11.

22.   Aparicio R, Rana A, Walker DW. Upregulation of the Autophagy Adaptor p62/SQSTM1

Prolongs Health and Lifespan in Middle-Aged Drosophila. Cell Rep 2019; 28:1029-1040.e5.

23. Kumsta C, Chang JT, Lee R, Tan EP, Yang Y, Loureiro R, Choy EH, Lim SHY, Saez I, Springhorn A, et al. The autophagy receptor p62/SQST-1 promotes proteostasis and longevity in C. elegans by inducing autophagy. Nat Commun 2019; 10:5648.

24. Burnett C, Valentini S, Cabreiro F, Goss M, Somogyvári M, Piper MD, Hoddinott M, Sutphin GL, Leko V, McElwee JJ, et al. Absence of effects of Sir2 overexpression on lifespan in C. elegans and Drosophila. Nature 2011; 477:482–5.

25. Hegedűs K, Nagy P, Gáspári Z, Juhász G. The putative HORMA domain protein Atg101 dimerizes and is required for starvation-induced and selective autophagy in Drosophila. Biomed Res Int 2014; 2014:470482.

26. Rana A, Oliveira MP, Khamoui A V., Aparicio R, Rera M, Rossiter HB, Walker DW. Promoting Drp1-mediated mitochondrial fission in midlife prolongs healthy lifespan of Drosophila melanogaster. Nat Commun 2017; 8:448.

27. Ciuffa R, Lamark T, Tarafder AK, Guesdon A, Rybina S, Hagen WJH, Johansen T, Sachse C. The Selective Autophagy Receptor p62 Forms a Flexible Filamentous Helical Scaffold. Cell Rep 2015; 11:748–58.

28. Mizushima N, Komatsu M. Autophagy: Renovation of cells and tissues. Cell 2011; 147:728–41.

29. Sasaki A, Nishimura T, Takano T, Naito S, Yoo SK. white regulates proliferative homeostasis of intestinal stem cells during ageing in Drosophila. Nat Metab 2021; 3:546–57.

30. Kageyama S, Gudmundsson SR, Sou Y-S, Ichimura Y, Tamura N, Kazuno S, Ueno T,

Miura Y, Noshiro D, Abe M, et al. p62/SQSTM1-droplet serves as a platform for autophagosome formation and anti-oxidative stress response. Nat Commun 2021; 12:16.

31. Sykiotis GP, Bohmann D. Keap1/Nrf2 Signaling Regulates Oxidative Stress Tolerance and Lifespan in Drosophila. Dev Cell 2008; 14:76–85.

32. Cornelissen T, Vilain S, Vints K, Gounko N, Verstreken P, Vandenberghe W. Deficiency of parkin and PINK1 impairs age-dependent mitophagy in Drosophila. Elife 2018; 7:1–14.

33. Mateju D, Franzmann TM, Patel A, Kopach A, Boczek EE, Maharana S, Lee HO, Carra S, Hyman AA, Alberti S. An aberrant phase transition of stress granules triggered by misfolded protein and prevented by chaperone function. EMBO J 2017; 36:1669–87.

34. Pircs K, Nagy P, Varga A, Venkei Z, Erdi B, Hegedus K, Juhasz G. Advantages and Limitations of Different p62-Based Assays for Estimating Autophagic Activity in Drosophila. PLoS One 2012; 7.

35. Deng H, Kerppola TK. Regulation of Drosophila Metamorphosis by Xenobiotic Response Regulators. PLoS Genet 2013; 9.

36. Jipa A, Vedelek V, Merényi Z, Ürmösi A, Takáts S, Kovács AL, Horváth G V., Sinka R, Juhász G. Analysis of Drosophila Atg8 proteins reveals multiple lipidation-independent roles. Autophagy 2021; 17:2565–75.

37. Takáts S, Nagy P, Varga Á, Pircs K, Kárpáti M, Varga K, Kovács AL, Hegedus K, Juhász G. Autophagosomal Syntaxin17-dependent lysosomal degradation maintains neuronal function in Drosophila. J Cell Biol 2013; 201:531–9.

Figure Legends

Figure 1. Knockin of a LIR mutation in *Drosophila* p62/Ref(2)P results in accumulation of polyubiquitinated protein aggregates.

(**A**) Schematic of *Drosophila* Ref(2)P showing the LIR (LC3-interaction region) and two amino acid substitutions (W454A, I457A) that disrupt the Ref(2)P-Atg8a interaction *in vivo*.

(**B**) Extracts from the indicated genotypes were subjected to immunoprecipitation with anti-RFP beads. Immunoprecipitated material (IP: mCherry) and corresponding crude lysates (Input) were run by SDS-PAGE and blotted for precipitated 3xmCherry-Atg8a forms (non-lipidated: I; lipidated: II as indicated) and co-precipitated endogenous Ref(2)P. *Atg16^{d67}* lysate additionally verifies the molecular weight of Ref(2)P, *w^{1118}* serves as negative control in the immunoprecipitation.

(**C**) Western blot of 3-day-old control, homozygous and heterozygous *Ref(2)P^{LIRm}* whole-fly lysates shows accumulation of Ref(2)P and polyubiquitinated proteins; α-tubulin: loading control. N=5 per genotype.

(**D**) Immunostaining of mid-L3 larval fat tissue reveal colocalization of poly-ubiquitin (FK2, green) and Ref(2)P (red) in mutants. Pearson's coefficients (*r*) are shown to indicate the extent of colocalization, DAPI (blue) labels nuclei. Bar: 2 μm.

(**E**) Quantification of the average number of Ref(2)P punctate structures from genotypes in panel C, N=6 for control; N=4 for *Ref(2)P^{LIRm}*. Statistical testing: unpaired two-tailed Student's t test. Error bars represent standard error. ** *p<0.01*.

(**F**) 3- and 30-day-old adult female brains of the indicated genotypes immunostained for poly-ubiquitin (green) and Ref(2)P (red) also show the striking overlap of these signals in mutants. N=4/genotype, bar: 10 μm.

(**G**) Ref(2)P-positive punctate structures in brains at the indicated ages and genotypes. Statistical testing: Kruskal-Wallis test with Bonferroni post-hoc test. Error bars mark standard error. *** $p<0.001$, ** $p<0.01$.

(**H**) Pearson's correlation coefficients (*r*) representing the level of colocalization between Ref(2)P and poly-ubiquitin in brains above threshold). Statistical testing: Kruskal-Wallis test with Bonferroni post-hoc test. Bars: standard error. ** $p<0.01$, * $p<0.05$.

(**I**) Electron micrographs of 3-day old cortical neuron cell-bodies from female control and *Ref(2)P^{LIRm}* animals showing membrane-less cytosolic aggregates in mutants (black arrows). Bar: 2 μm.

(**J**) Immunostaining for Ref(2)P in the brain of 3-day old female *Atg16^{d129}* and *Ref(2)P^{LIRm};Atg16^{d129}* mutant animals showing no difference in Ref(2)P aggregation. N=4/genotype, bar: 10 μm.

(**K**) Quantification of Ref(2)P puncta number from (J). Statistical testing: unpaired two-tailed Student's t test, $p>0.05$.

Figure 2. *Ref(2)P^{LIRm}* mutation has minimal effects on fly lifespan, while it results in increased resistance to oxidative stress.

(**A**) Lifespan analysis of *Ref(2)P^{LIRm}* flies compared to control. N=191, control; N=200, *Ref(2)P^{LIRm}*. Statistical testing: Kaplan-Meier survival analysis followed by Log-rank test.

(**B**) Complete starvation response in *Ref(2)P^{LIRm}* flies compared to control. N=112, control; N=110, *Ref(2)P^{LIRm}*. $p > 0.05$. Statistical testing: Kaplan-Meier survival analysis followed by Log-rank test.

(**C**) Climbing performance of 3- and 30-day old control and *Ref(2)P^{LIRm}* flies. N=300; 3-day old control and 3-day old *Ref(2)P^{LIRm}*; N=261, 30-day old control; N=269, 30-day old *Ref(2)P^{LIRm}*. Statistical testing: two-sided Mann-Whitney U test. Error bars=standard error. n.s.=not significant.

(**D**) Survival analysis of 3-day-old flies, which were fed with 20 mM PQ every 12 h until dead. N=314, control; N=337, *Ref(2)P^{LIRm}*. Statistical testing: Kaplan-Meier survival analysis followed by Log-rank test.

Figure 3. Keap1 sequestration in *Ref(2)P^{LIRm}* flies leads to activation of the CncC/Nrf2 pathway.

(**A**) 3-day-old adult female brains of indicated genotypes were immunostained for Ref(2)P and GFP-Keap1, showing partial colocalization (arrows) in *Ref(2)P^{LIRm}* flies in the optic lobe region. Bar: 10 μm. Pearson's coefficients (*r*) are indicted in insets. N=4 for both genotypes.

(**B**) Quantification of GFP-Keap1 puncta in the brain in the optic lobe region from genotypes in panel (A). Statistical testing: two-way Mann-Whitney U test. Bars: standard error. *** $p < 0.005$.

(**C**) Western blotting was performed for endogenous dmKeap1 from whole-fly lysates, using α-tubulin as loading control. Black arrow points to the specific band.

(**D**) Quantification of dmKeap1 western blot data from biological triplicates using unpaired two-tailed Student's t-test.

(**E**) The mRNA expression of *Ref(2)P*, *Keap1*, *GstE1*, *CncC*, *cat* and *GclC* was measured by Q-PCR and normalized to control. Statistical testing: two-sided Mann-Whitney U test. Bars: standard error. **** $p<0.0001$, *** $p<0.005$, ** $p<0.01$, * $p<0.05$, n.s., not significant.

(**F**) Mid-L3 larval anterior midgut from *tub*>GFP-CncC expressing animals of the indicated genotypes was dissected and imaged immediately. Bar: 50 μm. N=6; *UAS-GFP-CncC/+;tub-Gal4/+* and *UAS-GFP-CncC/+; Ref(2)P^{LIRm}; tub-Gal4/+*.

(**G**) Cytosolic GFP fluorescence was calculated by subtracting GFP fluorescence in the nucleus (ROI selection from DAPI staining; orange circles in panel F) from the whole cell (cyan in panel F), and subsequently nuclear GFP fluorescence was divided by cytosolic GFP fluorescence to get the nucleus/cytoplasm fluorescence ratio. Cells quantified: N=66, control; N=62, *Ref(2)P^{LIRm}*. Statistical testing: two-sided Mann-Whitney U test. Bars: standard error. **** $p<0.0001$.

(**H**) Paraquat survival response of *Ref(2)P^{LIRm}* flies with or without CncC RNAi reveals that oxidative stress resistance requires CncC/Nrf2. 3-day-old female flies were fed with 20 mM PQ every 12 h and the number of flies alive was recorded. N=314, control; N=172, *tub-Gal4/CncC-IR^{TRiP.HMS00650}*; N=337, *Ref(2)P^{LIRm}*; N=149, *Ref(2)P^{LIRm};tub-Gal4/CncC-IR^{TRiP.HMS00650}*. Statistical testing: Kaplan-Meier survival analysis followed by Log-rank test.

Figure 4. Increased mitochondrial superoxide production during aging is ameliorated in *Ref(2)P^{LIRm}* flies.

(**A**) Whole brains of 45-day-old adult females of the indicated genotypes were dissected and dual-stained with Mitosox Red (labels mitochondrial superoxide) and Mitotracker Green FM (MTG; labels mitochondria) as described in Methods. Cells from optic lobe were imaged. Scale bar: 10 μm.

(**B**) Quantification of Mitosox Red data from panel (A). Regions of interest containing consistent DAPI signal from each image were selected for measurement of Mitosox fluorescence intensity per unit area. N=6 for control and *Ref(2)P^{LIRm}, tub-Gal4/CncC-IR$^{TRiP.HMS00650}$ and Ref(2)P^{LIRm};tub-Gal4/CncC-IR$^{TRiP.HMS00650}$*. Statistical testing: two-sided Mann-Whitney U test. **** $p<0.0001$. n.s.=not significant.

Figure 5.

(**A**) L3-mid larval fat tissue was dissected and immunostained for Ref(2)P and ubiquitin (FK2). N=6, *UAS-GFP-Ub,tub-Gal4/TM6, Ref(2)P^{LIRm}* and *Ref(2)P^{LIRm}; UAS-GFP-Ub,tub-Gal4/TM6*. Colocalization examples are shown in insets.

(**B**) Size of individual Ref(2)P aggregates. Statistical testing: two-sided Mann-Whitney U test. **** $p<0.0001$.

(**C**) Number of Ref(2)P aggregates per cell. Statistical testing: two-way unpaired Student's t test. ****$p<0.0001$, *$p<0.05$.

(**D**) Number of Ref(2)P only puncta divided by Ref(2)P puncta having ubiquitin signal. Statistical testing: two-way unpaired Student's t test (Ref(2)P^{LIRm} vs. Ref(2)P^{LIRm}, *tub*-GFP-Ub), ****$p<0.0001$; two-way Mann-Whitney U test (*tub*-GFP-Ub vs. Ref(2)P^{LIRm}, *tub*-GFP-Ub), n.s.=not significant.

(**E**) CCCP-induced mitophagy in fat tissue immunostained for Ref(2)P and ATP5a (mitochondrial marker). N=6, w^{1118}, *Ref(2)P^{LIRm}* and *Ref(2)P^{LIRm}; UAS-GFP-Ub/tub-Gal4*. Colocalizations are shown in insets.

(**F**) Quantification of mitophagy events (Ref(2)P puncta positive for ATP5a signal).

(**G**) Loss of LIR-mediated recognition of ubiquitinated cargo in autophagosomes results in cargo sequestration in p62 bodies while bulk autophagy is unaffected. Activation of Nrf2/CncC via Keap1 inhibition as well as sequestration of potentially cytotoxic cargo in these p62 bodies lead to upregulated cellular antioxidant response and reduced mitochondrial superoxide levels during aging. Expression of GFP-Ub disrupts Ref(2)P aggregate formation and redirects Ref(2)P to mitochondria during mitophagic induction.

Figure 1

A

core LIR

Ref(2)P   451   DPEWQLIDN   459

Ref(2)P   DPEWQLIDN   459
SQSTM1/p62   DDDWTHLSS   343

HP1   HP2

Atg8a/LC3

Ref(2)P^LIRm   DPEAQLADN

Atg8a/LC3

B

Input   IP: mCherry

130 —
100 —   ← Ref(2)P

100 —   I   3xmCherry-
          II   Atg8a-

C

Ref(2)P
Line 1   Line 2

100 —   Ref(2)P

250 —
130 —   Ubiquitin
100 —

55 —   α-Tub.

D   L3-mid larval fat tissue

Control   r=0.19
Ub.   Ref(2)P   merge+ DAPI

Ref(2)P^LIRm   r=0.80

E   L3-mid larval fat tissue

F   Adult brain

Control   Ref(2)P^LIRm

G   Ref(2)P-positive aggregates/unit area

H   Pearson's r (Ref(2)P/Ubiquitin)

I   adult cortical neuron

Control   Ref(2)P^LIRm

J   Adult brain, 3 day

Ref(2)P
Atg16^d129

Ref(2)P^LIRm; Atg16^d129

K   Ref(2)P puncta/unit area

n.s.

Figure 2

Figure 3

A | Adult brain, optic lobe, 3-day old

nSyb>GFP-Keap1

Ref(2)P

r=0.07

Control

r=0.62

Ref(2)P^{LIRm}

B

GFP-Keap1 puncta /unit area

● Control
▼ Ref(2)P^{LIRm}

***

C | whole fly lysate, 3-day old

Control   Ref(2)P^{LIRm}

100
70 — ◄ dmKeap1
55 — α-Tub.

D

dmKeap1 /α-Tub (A.U.)

*

Control   Ref(2)P^{LIRm}

E

Relative mRNA

Control

n.s. **** * ** *** n.s.

Ref(2)P *Keap1* *GstE1* *CncC* *Cat* *GclC*

F | L3-mid larval ant. midgut

Control   Ref(2)P^{LIRm}

tub>GFP-CncC

G

Mean GFP nucl./ cyto. fl. (A.U.)

****

Control   Ref(2)P^{LIRm}

H

Probability of survival

PQ fed

Time (hr.)

Control
tub>CncC.RNAi
Ref(2)P^{LIRm}
Ref(2)P^{LIRm}, *tub*>CncC.RNAi

*
****

Figure 4

A

| Brain, optic lobe, 45 day |

Control

Ref(2)P^LIRm

tub>CncC.RNAi

Ref(2)P^LIRm,
tub>CncC.RNAi

merge+DAPI   MTG   Mitosox Red   10 μm

B

Mean Mitosox red fl. intensity (A. U.)

0.6

0.4

0.2

0.0

Control   Ref(2)P^LIRm   *tub*>CncC.RNAi   Ref(2)P^LIRm, *tub*>CncC.RNAi

****   n.s.   ****

Figure 5

A — L3-mid larval fat tissue

merge+ DAPI
tub>GFP-Ub
Ref(2)P
Ub.
Ref(2)P^{LIRm}
Ref(2)P^{LIRm}; *tub*>GFP-Ub
10 µm
2 µm

B Ref(2)P puncta size (µm^2)
****
tub>GFP-Ub
Ref(2)P^{LIRm}
Ref(2)P^{LIRm}; *tub*>GFP-Ub

C Ref(2)P puncta number
*
tub>GFP-Ub
Ref(2)P^{LIRm}
Ref(2)PLIRm; tub>GFP-Ub

D Ref(2)P+/ Ref(2)P+Ub+ puncta
****
tub>GFP-Ub
Ref(2)P^{LIRm}
Ref(2)P^{LIRm}; *tub*>GFP-Ub

E — L3-mid larval fat tissue, CCCP, 200 µM

merge+ DAPI
Control
Ref(2)P
ATP5a
Ref(2)P^{LIRm}
Ref(2)P^{LIRm} *tub*>GFP-Ub
10000 nm
5 µm

F ATP5α positive Ref(2)P puncta
**
Control
Ref(2)P^{LIRm}
Ref(2)P^{LIRm}; *tub*>GFP-Ub

G

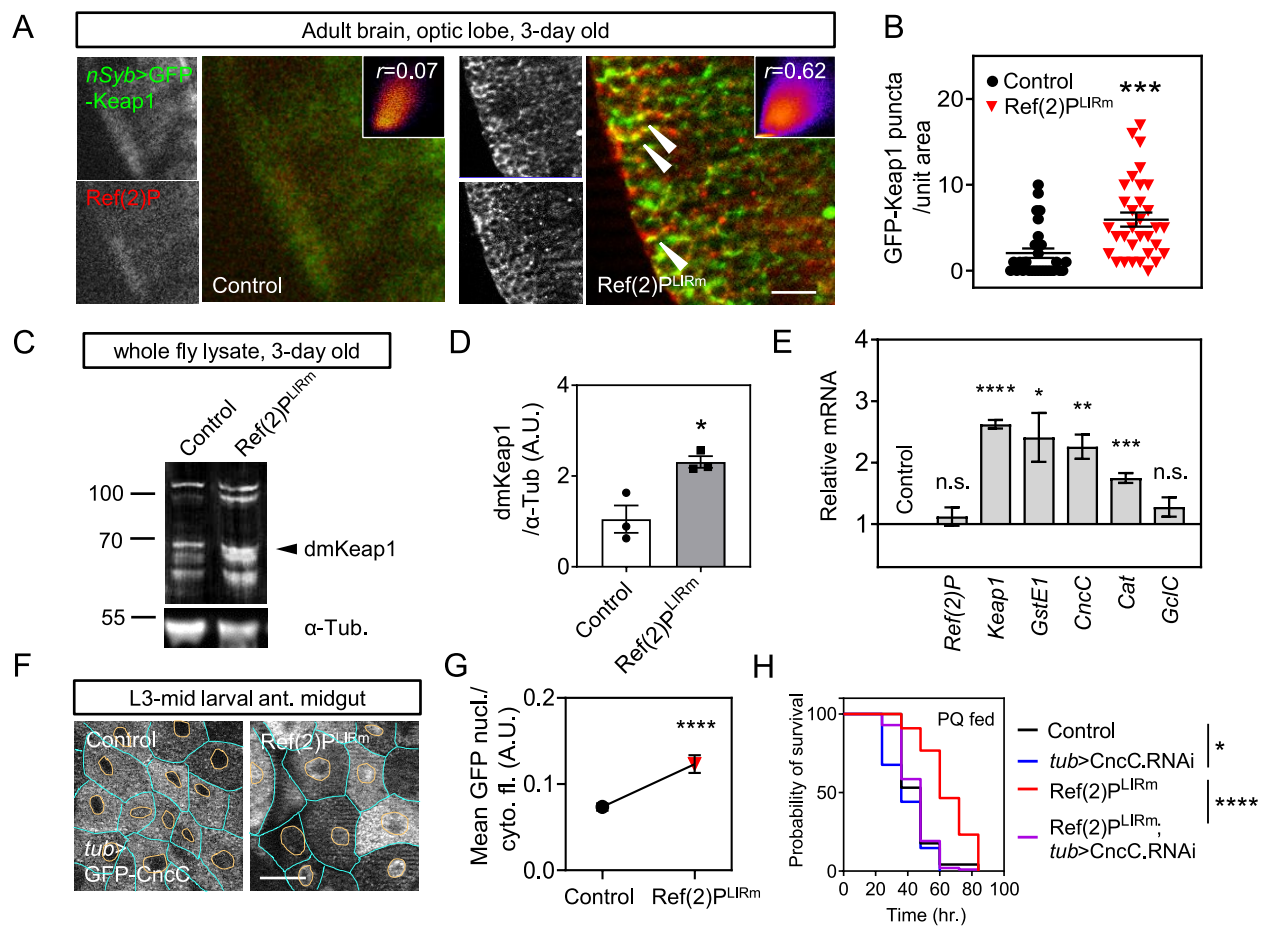|			
Ref(2)P^{wt}	No ubiquitinated cargo accumulation	Low basal CncC/Nrf2 activity	High mitochondrial superoxide during aging
Ref(2)P^{LIRm}	Ub-Keap1-Ref(2)P Co-accumulation	High basal CncC/Nrf2 activity	Low mitochondrial superoxide during aging
Ref(2)P^{LIRm}	No disruption of aggregates	Mitophagy induction (CCCP)	Low Ref(2)P mito. localization
tub>Ub	Partial disruption of aggregates		High Ref(2)P mito. localization

Supplementary Figure Legends

Supplementary Figure S1
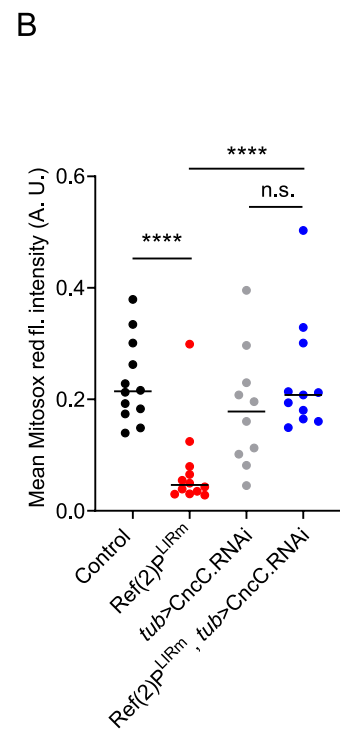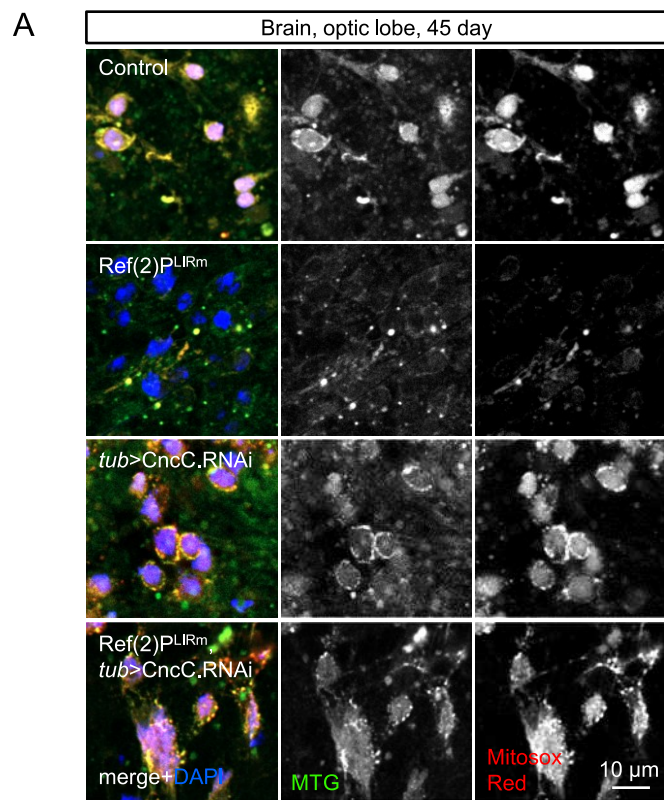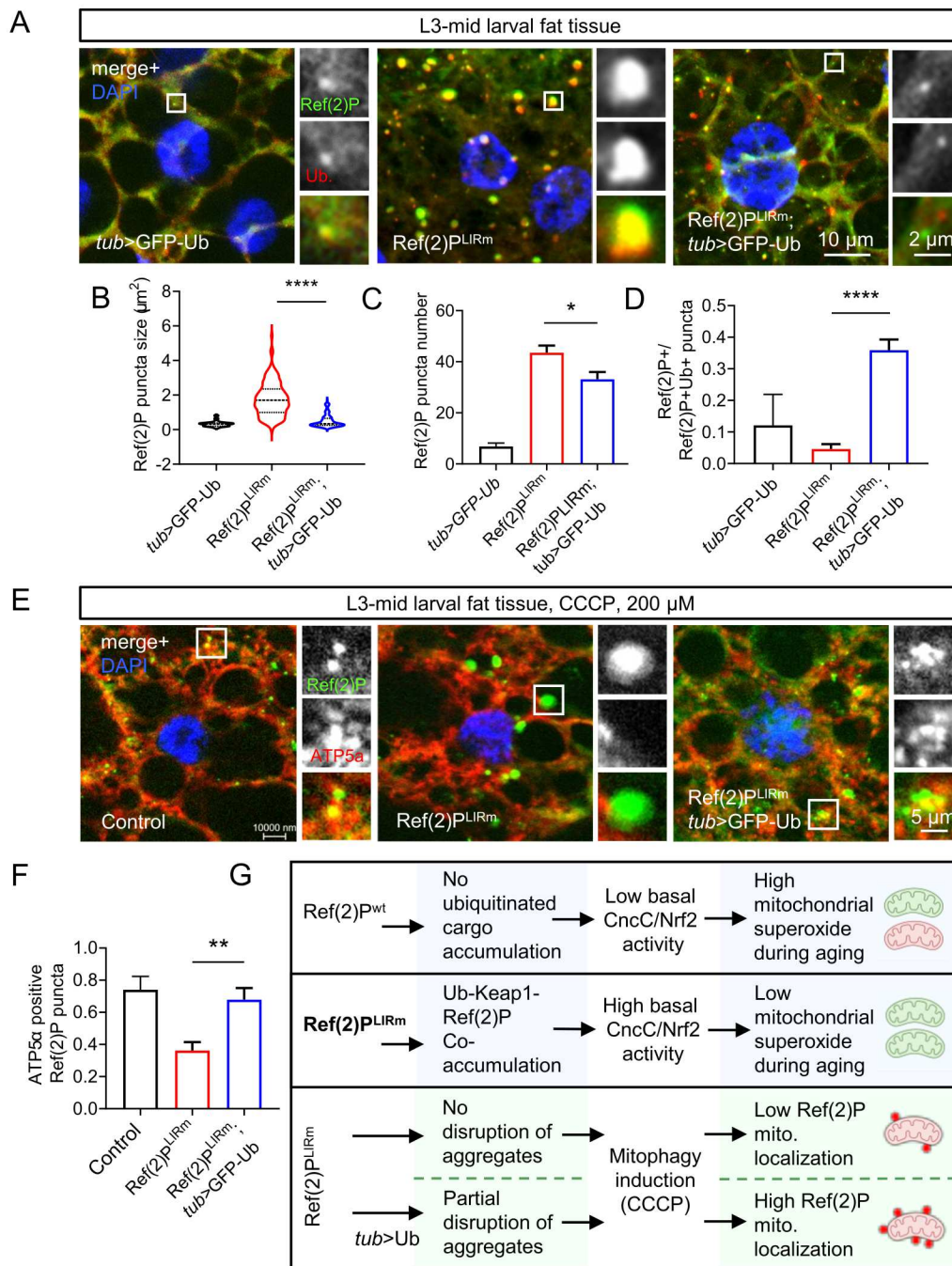
Click here to access/download
Supplementary Material - for review
S1.eps

Click here to access/download
Supplementary Material - for review
S2.eps

Click here to access/download
**Supplementary Material - for review
S3.eps**

Click here to access/download
**Supplementary Material - for review
S4.eps**

Click here to access/download
Supplementary Material - for review
S5.eps